NeuroImage: Clinical 19 (2018) 417–424

Contents lists available at ScienceDirect

NeuroImage: Clinical

journal homepage: www.elsevier.com/locate/ynicl

Baseline biomarkers of connectome disruption and atrophy predict future processing speed in early multiple sclerosis

A. Kuceyeski[a,c,*], E. Monohan[b], E. Morris[b], K. Fujimoto[b], W. Vargas[b], S.A. Gauthier[b,c]

[a] Department of Radiology, Weill Cornell Medicine, New York, NY, USA
[b] Department of Neurology, Weill Cornell Medicine, New York, NY, USA
[c] The Feil Family Brain and Mind Research Institute, Weill Cornell Medicine, New York, NY, USA

ARTICLE INFO

Keywords:
Multiple sclerosis
Connectome
White matter
Follow-up studies
Atrophy
Cognition
Prognosis

ABSTRACT

The development of accurate prognoses in multiple sclerosis is difficult, as the disease is characterized by heterogeneous patterns of brain abnormalities that relate in an unclear way to future impairments. Here, we use a statistical modeling approach to determine if the baseline pattern of connectome disruption due to T2-FLAIR lesions could predict a patient's future processing speed, as measured using the Symbol Digits Modality Test scores. Imaging data, demographics and Symbol Digits Modality Test scores were collected from 61 early relapsing remitting multiple sclerosis patients. The Network Modification Tool was used to estimate damage to the connectome by quantifying white matter abnormalities' effects on 1) global network properties, 2) regional connectivity and 3) connectivity between pairs of regions. MS subjects showed significant improvement of processing speed between baseline and follow-up ($t = -2.6$, $p = 0.0096$); however, both baseline ($t = -4.01$, $p = 0.00012$) and follow-up ($t = -2.10$, $p = 0.038$) processing speed were significantly lower than age-matched healthy controls. Partial Least Squares Regression was used to create models that predict future processing speed from between baseline imaging metrics and demographics. The model based on region-pair disconnection and gray matter atrophy had the lowest AIC and highest prediction accuracy ($R^2 = 0.79$) compared to models based on global ($R^2 = 0.41$) or regional ($R^2 = 0.66$) disconnection and gray matter atrophy, overlap with an ROI-based atlas and gray matter atrophy ($R^2 = 0.73$) or gray matter atrophy alone ($R^2 = 0.71$). We found that baseline measures of connectivity disruption in various parietal, temporal, occipital and subcortical regions and atrophy in the putamen were important predictors of future processing speed. We conclude that information about disruptions to pairwise brain connections is more informative of future processing speed than regional or global metrics or gray matter atrophy alone. The combination of quantitative disconnectome metrics, gray matter atrophy and statistical modeling approaches could enable clinicians in developing more accurate, individualized prognoses of future cognitive status in multiple sclerosis patients.

1. Introduction

The increased availability of neuroimaging data sets from clinical populations provides many opportunities for gaining a deeper understanding of brain anatomy and physiology. One important, clinically-relevant goal is to better understand how pathological brain abnormalities map to impairments and how the brain compensates for these abnormalities in recovery. The former information would help in developing more accurate prognoses and the latter would help in developing effective treatments. One disease that could provide a unique opportunity for understanding such brain-behavior relationships is multiple sclerosis (MS). MS is a disease associated with focal lesions mostly in the white matter (WM) and some in gray matter (GM) and cortical/subcortical atrophy that result in impairments of sensory-motor function, vision and cognition. The spatial and temporal pattern of MS lesions is heterogeneous across both patients and over time, and the impact of said lesions on current and future impairment is not well-known. Quantifying brain-behavior relationships and how they evolve over time is crucial in developing accurate prognoses and provides insight as to how the brain recovers from disease-related damage.

WM pathology and structural networks have been studied extensively in MS (Rocca et al., 2012; Shu et al., 2011), with many studies using tractography methods (Hu et al., 2011; Mesaros et al., 2012). However, tractography is not always clinically feasible as it is onerous, requires a high level of expertise and can be particularly challenging in pathology (Jones and Cercignani, 2010) due to decreased signal-to-

* Corresponding author at: Weill Cornell Medical College, 425 East 61st St, New York, NY 10065, USA.
E-mail address: amk2012@med.cornell.edu (A. Kuceyeski).

https://doi.org/10.1016/j.nicl.2018.05.003
Received 7 March 2018; Received in revised form 4 May 2018; Accepted 6 May 2018
Available online 08 May 2018

noise ratio in the diffusion MRI (Kuceyeski et al., 2011; Pagani et al., 2007; Pierpaoli et al., 2001; Wheeler-Kingshott and Cercignani, 2009). In place of using tractography in the patient, we propose using The Network Modification (NeMo) Tool (Kuceyeski et al., 2013). The NeMo Tool can be used to estimate global, regional and network-level structural connectivity losses from a WM abnormality mask only; it does not require performing tractography or even diffusion MRI in patient populations. We previously applied the NeMo Tool to a similar dataset of MS patients and found that a moderate amount of baseline processing speed impairment ($R^2 = 0.42$) could be explained by baseline regional GM atrophy and regional disconnection scores (Kuceyeski et al., 2015a).

Here, in the spirit of clinical relevancy, our goal is to predict future processing speed from baseline imaging of GM atrophy as well as global, regional and region-pair disconnection measures derived from the NeMo Tool. We hypothesize that considering an MS patient's specific pattern of pathology and quantifying how that pattern disrupts structural connections can be used to predict future neurological outcomes and disease progression. We use Partial Least Squares Regression (PLSR) to relate baseline imaging biomarkers of disconnection and GM atrophy to future processing speed. Our goals are to 1) identify which of our five models (based on GM atrophy, global, regional and region-pair disconnectivity and atlas overlap) has the best accuracy in predicting follow-up processing speed and to 2) identify which of the global/regional/pairwise disconnectivity, atrophy and atlas overlap metrics in these models are significant predictors of future processing speed. To the author's knowledge, this is the first study that uses baseline structural disconnectivity metrics and GM atrophy biomarkers to predict future cognitive changes in early MS.

2. Materials and methods

2.1. Subjects

Data was collected from 61 early relapsing-remitting MS patients (Table 1). Study procedures were explained to and consent was obtained from subjects in this IRB-approved study. All but three patients were on disease modifying therapies for MS at the time of MRI, with average treatment duration of 0.5 ± 0.9 years. All patients' baseline MRIs were acquired within 5 years of their first neurologic symptom. Three sets of images were acquired on a 3 T GE scanner (HDxt 16.0) using 8-channel phased-array coil: T1-weighted sagittal 3D-BRAVO ($1.2 \times 1.2 \times 1.2$ mm), T2 ($0.5 \times 0.5 \times 3$ mm) and T2-FLAIR ($1.2 \times 0.6 \times 0.6$ mm). The written version of the Symbol Digits Modality Test (SDMT), which measures processing speed, was performed on this cohort at baseline and on average 28.6 ± 10.3 months follow-up. Processing speed is one of the earliest cognitive domains affected in MS and the SDMT is particularly sensitive to this type of impairment (Bergendal et al., 2007).

Table 1
Subject demographics.

	MS subjects ($N = 60$)	Normal Controls ($N = 14$)
Age	36.8 ± 9.3 years	37.3 ± 13.3
Sex M/F	16/44	5/9
Disease Duration	1.5 ± 1.3 years	N/A
Treatment Duration	0.5 ± 0.9 years	N/A
Baseline EDSS	1.1 ± 1.1	N/A
Baseline SDMT	48.1 ± 11.5	N/A
Follow-up SDMT	53.3 ± 9.9	N/A
Time between baseline and follow-up SDMT	28.6 ± 10.3 months	N/A

2.2. T2-FLAIR hyperintensity lesion masks

Lesion masks were created as in our previous work (Kuceyeski et al., 2015a). As in that work, FreeSurfer (Dale et al., 1999; Fischl et al., 1999) was used on the T1 images to create tissue segmentations and subcortical and cortical parcellations, which were manually edited for misclassification due to hyperintensities in WM and temporal region errors. The T2 FLAIR images were linearly coregistered to the T1, masked with the WM and subcortical masks and thresholded to create a preliminary WM abnormality mask. The preliminary WM abnormality mask was then manually edited using the T2 and T2 FLAIR overlay and final approval given by a trained neurologist. T1 images were also acquired on 14 age-matched healthy volunteers and processed with the same pipeline to produce cortical thicknesses for calculating GM atrophy (see Table 1).

2.3. The NeMo tool

The NeMo Tool can be used to estimate changes to the structural connectivity network that result from a particular pattern of WM pathologies by referencing a database of 73 normal control tractograms in a common space (Montreal Neurological Institute). MS subjects' WM abnormality masks were normalized to MNI space using first a linear coregistration followed by non-linear normalization in SPM8. The atlas used within the NeMo Tool was derived from FreeSurfer, with 68 cortical regions, 16 subcortical and 2 cerebellar structures. Pairwise disconnection measures are identified by removing those streamlines passing through the WM abnormality mask and recalculating the strength of connections between pairs of regions, resulting in the "modified connectome". Global metric changes are estimated by calculating graph-theoretic metrics, i.e. efficiency, characteristic path length, clustering coefficient and betweenness centrality, on this modified connectome. Regional disconnectivity changes are estimated via the Change in Connectivity (ChaCo) score that is the percent of tracts that pass through the WM abnormality mask for a given GM region. The NeMo Tool calculates one "modified connectome", associated global connectome measures and set of ChaCo scores for each of the 73 controls and reports the average over these values. We use the average value as input to our predictive models. We also calculate the z-scores of the pairwise connections in each subject's "modified connectome" compared against the 73 control connectomes in the NeMo Tool to identify which region-pairs had the most disconnection. The number of lesions a tract passes through is not considered; tracts removal was a binary process. To compare an imaging metric not related to connectivity, we also calculated the overlap of the WM abnormality masks with the JHU-MNI "Eve" atlas of 176 gray and white matter regions. For each region in the atlas, the percent of voxels in the region within the lesion mask was calculated. Finally, atrophy was measured by calculating standard z-scores of average thickness for 68 cortical regions, volume for 16 subcortical regions and 2 cerebellar regions from the FreeSurfer atlas, using a group of 14 age- and sex-matched normal controls (see Table 1) that had the same scans and pre-processing. The 86-region atlas used in the NeMo Tool (global network metrics, ChaCo scores and pairwise disconnection measures) and for GM atrophy measures was identical.

2.4. Partial least squares regression

The modeling approach used here is similar to the work done in our previous paper that predicted baseline SDMT from baseline imaging metrics (Kuceyeski et al., 2015a). PLSR models were constructed to predict follow-up SDMT based on a subject's age, sex, disease duration, treatment duration, baseline SDMT, baseline EDSS, number of months between time points, regional GM atrophy and one of four imaging metrics: three levels of connectivity disruption metrics from the NeMo Tool (global, regional and pairwise disconnection measures) and the

JHU-MNI atlas-overlap metric. The global model included overall lesion volume, mean GM atrophy, and the global connectome measures of characteristic path length, efficiency, clustering coefficient and betweenness centrality. The regional model included 86 ChaCo scores for each GM region and the pairwise disconnection model included 610 pairwise connections out of $(86 \times 85)/2 = 3655$ possible. There is some variation in the presence of edges across individuals due to population variability, noise present in imaging and post-processing, etc. In order to focus on region-pairs that have the highest probability of connection, we chose to include only those 610 edges that were non-zero in all 73 normal controls. One of the goals of this work is to assess the relative contributions of the various disconnection and atlas-overlap metrics, which is why we have one model built for each of the measures. Two other models, one using only demographics (no imaging) and one using demographics and regional GM atrophy, were also calculated for assessment of how much more variance is explained by adding each of the other imaging metrics to the prediction.

PLSR is useful when analyzing data with more explanatory variables than observations ($p \gg n$), as the data are reduced to highly relevant and mutually independent components. PLSR performs dimensionality reduction by creating new variables (components) from the original data that have maximal correlation with the outcome, followed by regression on those new components. In addition, the components are guaranteed to be mutually independent even if the input variables are co-linear. K-fold cross-validation ($k = 10$) was performed to identify the number of components that minimized the predicted residual sum of squares (PRESS) on the hold-out set over 50 different partitions. The cross-validation procedure was performed over 1000 bootstrapped sets and the number of components that most frequently minimized PRESS was identified. Once the number of components was set, bootstrapping of 50,000 samples with replacement was performed (Krishnan et al., 2011) and confidence intervals (CIs) derived for the regression coefficients of the model via the bias-corrected and accelerated percentile method (Efron, 1987). CIs were corrected for multiple comparisons over the number of input variables within each model using Bonferroni correction (Bonferroni, 1936). If the adjusted CI for an input variable did not include zero, it was considered a significant predictor. PLSR coefficients for the brain regions and region-pairs were illustrated via glassbrains created using Brainography (LoCastro et al., 2014).

The four models were compared via R^2 values, root mean squared error and Akaike Information Criterion (AIC) (Burnham and Anderson, 2002), the latter of which measures goodness-of-fit while considering model complexity. AIC is used to compare the models, as it allows comparison of non-nested models while accounting for the number of input variables. The difference in AIC for model i from the minimum AIC across all models ($\Delta_i = AIC_i - \min AIC$) provides relative comparison of models that have a different of input variables. Generally, $\Delta_i < 2$ indicates substantial evidence for the model, $2 < \Delta_i < 7$ indicates less support while $\Delta_i > 10$ indicates that the model is unlikely. Akaike weights, i.e. $w_i = \exp(-\Delta_i/2)/\Sigma_M \exp(-\Delta_i/2)$, were calculated for the $M = 4$ models and provided the probability that the model is the best among all candidate models (Burnham and Anderson, 2002). All models and statistical tests were performed in Matlab.

3. Results

3.1. Longitudinal SDMT

Fig. 1A shows box-and-whisker plots of the SDMT scores at baseline and follow-up, where a single line represents each individual. Red lines indicate a patient whose SDMT decreased (got worse) beyond minimal clinically important difference (MCID), gray for stable patients and green for those patients whose SDMT scores increased (got better) beyond MCID. Here, we consider MCID to be 4 points, as suggested by Benedict et al. (2017). SDMT scores showed significant improvement between baseline and follow-up (two-tailed paired t-test, $t = -2.6$, $p = 0.0096$), see Fig. 1A. SDMT scores were significantly lower than a previously published age-matched normal control population (Bate et al., 2001) at both baseline (two-tailed unpaired t-test: $t = -4.01$, $p = 0.00012$) and follow-up (two-tailed unpaired t-test: $t = -2.10$, $p = 0.038$). There was a moderate, significant partial Pearson's correlation between baseline SDMT and change in SDMT after controlling for time between baseline and follow-up and age ($r = -0.61$, $p = 2.8 \times 10^{-7}$, see scatter plot in Fig. 1B). Note: one subject had an extremely large amount of WM damage over the whole brain relative to the rest of the population (i.e. the z-score of the average ChaCo score was > 5) and was excluded from all of the analyses.

3.2. Disconnection scores, atlas overlap and atrophy patterns

Fig. 2 summarizes the NeMo Tool's three levels of disconnection metrics: A) global network metrics, B) ChaCo (regional) disconnection scores and C) pairwise disconnection scores. Overall, the global metrics (Fig. 2A) did not change drastically, with betweenness centrality and clustering coefficient showing marginal decreases and efficiency and characteristic path length essentially unchanged. Fig. 2B shows the regional disconnection (ChaCo) scores, with parietal and cingulate areas showing the most disconnection (see Supplemental Table I). In particular, the bilateral caudate nucleus, superior/inferior parietal gyri, pericalcarine, caudal anterior cingulate, putamen, left posterior cingulate, left caudal middle frontal gyrus, right paracentral and left precentral showing the most disconnection. Fig. 2C shows the z-scores of the pairwise disconnection measures for the entire connectome. Fig. 2B and C are arranged/labeled by functional assignment based on the Yeo atlas (Yeo et al., 2011). Each region in our 86-region FreeSurfer derived atlas was assigned to one of the 8 functional areas in the Yeo atlas by majority voxel vote, i.e. the region was assigned to the most frequently occurring functional label within its voxels. Subcortical structures, dorsal and ventral attention, somato-motor and default mode areas were most affected (see Supplemental Table II for the top 100 most disconnected region-pairs).

Fig. 3A illustrates the mean atrophy over the 86-region atlas, with regions smaller than controls in red and regions larger than controls in blue. Areas of highest atrophy included mainly subcortical areas (putamen and thalamus) and temporal regions, including the entorhinal and hippocampal areas (see Supplemental Table III). The median of the atlas overlap metric for the 176-region JHU-MNI “Eve” atlas is illustrated in Fig. 3B, with GM regions in gray and WM regions in black. White matter regions were most affected, particularly the bilateral tapetum (part of the corpus callosum), thalamic radiation, posterior/superior corona radiata, splenium and body of the corpus callosum (see Supplemental Table IV).

3.3. Regression results

The results from the regression techniques are summarized in Fig. 4 and Table 2. The top part of each panel shows the model predictions versus the observed SDMT with the corresponding R^2 value in the upper left corner. The bottom part of each panel illustrates the regression coefficients for each of the models, where the magnitude of the region/connection's coefficient determines the radius of the sphere/pipe. Bright and light blue indicate those regions/connections whose disconnection was related to worse follow-up SDMT, with the variables that had CIs not including 0 in bright blue and the ones that did include 0 in light blue. Red and pink indicate those regions/connections whose disconnection was related to better follow-up SDMT, with the variables that had CIs not including 0 in red and the ones that did include 0 in pink. A comprehensive list of the variables identified as significant by PLSR and their regression estimates are given in Supplemental Table V.

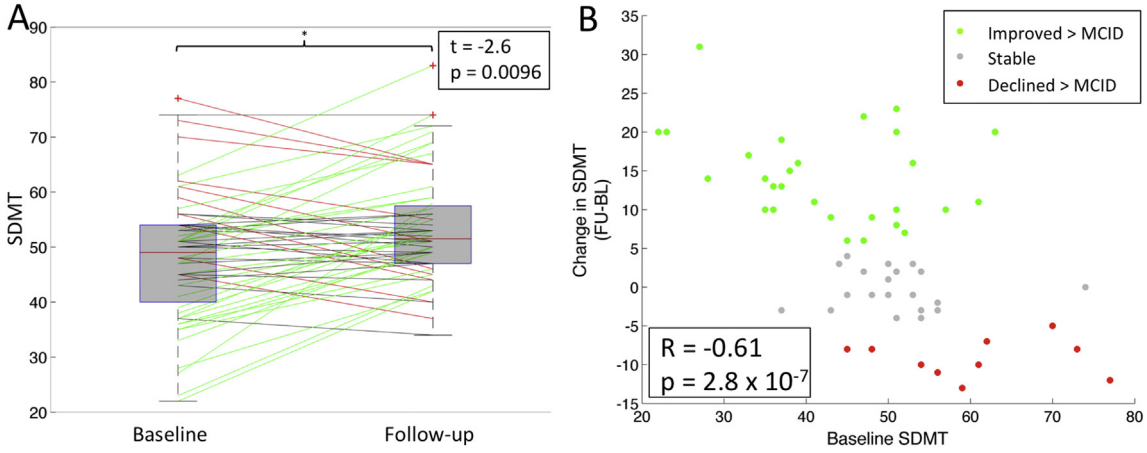

Fig. 1. Longitudinal SDMT. A) Boxplots of the baseline and follow-up SDMT ($t = -2.6$, $p = 0.0096$) and B) A scatter plot of the baseline SDMT versus change in SDMT (partial Pearson's $R = -0.61$, $p = 2.8 \times 10^{-7}$, controlling for time between visits and age). Red lines/points indicate patients with longitudinal decreases in SDMT beyond minimal clinically important difference (MCID), gray lines/points are longitudinally stable patients and green lines/points indicate patients with longitudinal increases in SDMT beyond MCID. (For interpretation of the references to color in this figure legend, the reader is referred to the web version of this article.)

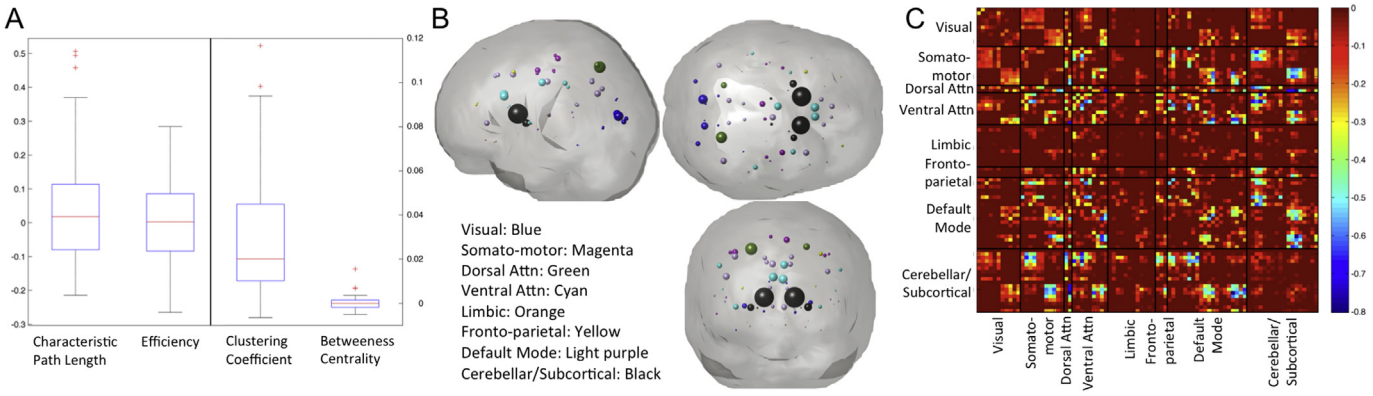

Fig. 2. Connectome disruption in early MS quantified using the NeMo Tool. A) Normalized difference in global connectome metrics for the MS patients compared to the metrics from the average normal connectome from the controls in the NeMo Tool. B) Average regional Change in Connectivity (ChaCo) scores for each of the 86 cortical and subcortical regions. C) The median of the z-score of the pairwise connectivity of the MS subjects compared to the normal controls in the NeMo Tool.

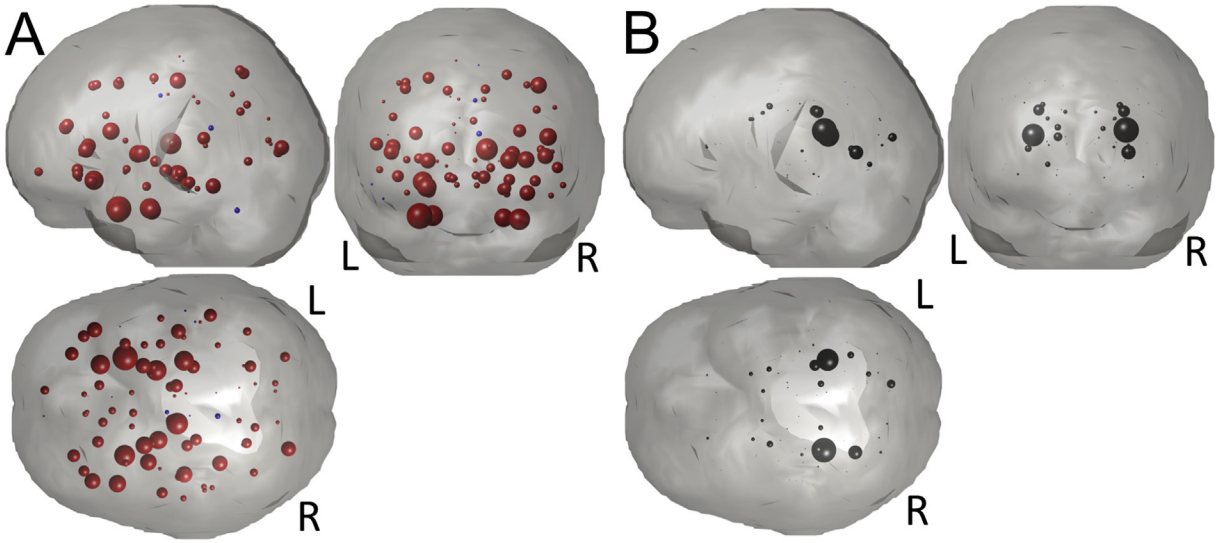

Fig. 3. Atrophy and lesion overlap in early MS. A) Mean z-scores of gray matter atrophy for the MS patients compared to the 14 age and sex matched healthy controls (red = regions showing cortical thinning or volume decreases, blue = regions showing cortical thickening or volumetric increases) B) Median lesion overlap metric using the 176 region Johns Hopkins University Atlas of white matter (in black) and gray matter (in gray) structures (larger radius = more overlap). (For interpretation of the references to color in this figure legend, the reader is referred to the web version of this article.)

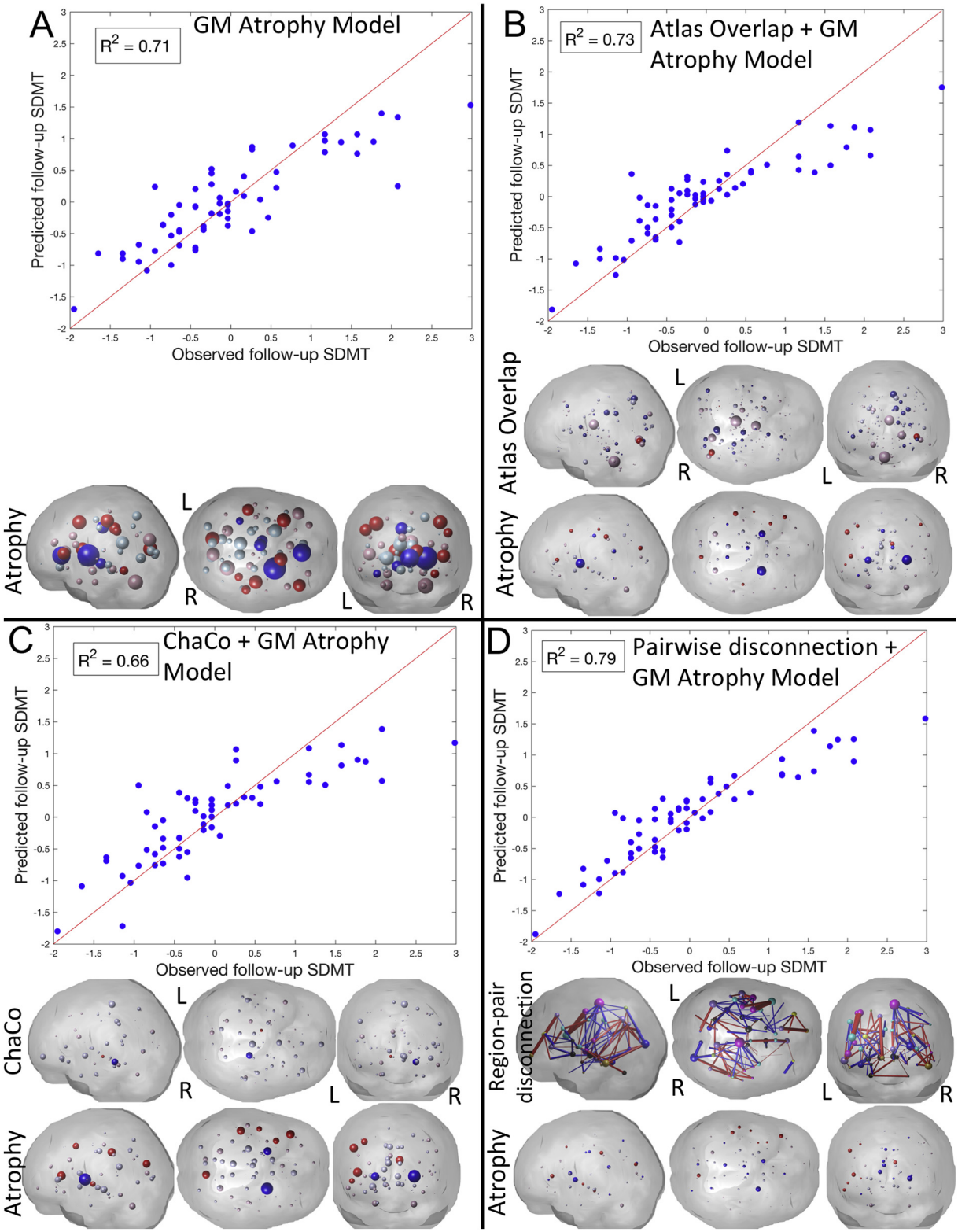

Fig. 4. Regression results. Predicted SDMT versus observed follow-up SDMT (top part of each panel) and EN regression coefficients (bottom part of each panel) for the models based on A) GM atrophy, B) ChaCo scores and GM atrophy, C) atlas overlap and GM atrophy and D) pairwise disconnection and GM atrophy. Blue spheres/pipes represent those regions/connections whose disconnection was related to worse follow-up SDMT scores, with bright blue indicating those that were included in the final stepwise regression model and light blue indicating those that were not. Red spheres/pipes indicate those regions/connections whose disconnection was related to better follow-up SDMT scores and were included in the final stepwise regression model. Regions (spheres) in Panel B are color coded by functional atlas assignment, as in Fig. 3 (visual = blue, somatomotor = magenta, dorsal attention = green, ventral attention = cyan, limbic = orange, fronto-parietal = yellow, default mode = light purple, cerebellar/subcortical = black). (For interpretation of the references to color in this figure legend, the reader is referred to the web version of this article.)

Table 2
Comparison of the PLSR models predicting SDMT from various MRI-based metrics and demographic variables. R^2, AIC, Δ_iAIC and w_i are based on the single model that is the mean of the PLSR coefficients over the bootstrapped samples.

Model	# Comp.	R^2	AIC (Δ_i AIC)	w_i	95% CI for R^2
Demographics Model: age, gender, disease duration, treatment duration, baseline SDMT, time between baseline and follow-up, baseline EDSS	1	0.35	−25.42 (59.85)	~0%	[0.13, 0.55]
Global Model: Demographics + Lesion Volume + Global GM Atrophy + Global Network Metrics	2	0.41	−29.55 (55.72)	~0%	[0.16, 0.58]
GM Atrophy Model: Demographics + Regional GM Atrophy	4	0.71	−67.95 (17.31)	0.017%	[0.67, 0.82]
Atlas-overlap and GM Atrophy Model: Demographics + Regional GM Atrophy + Atlas Overlap	4	0.73	−72.29 (12.97)	0.15%	[0.67, 0.88]
ChaCo and GM Atrophy Model: Demographics + Regional GM Atrophy + Regional Disconnection (ChaCo)	4	0.66	−59.01 (26.26)	0.00019%	[0.57, 0.78]
Pairwise Disconnection and GM Atrophy Model: Demographics + Regional GM Atrophy + Pairwise disconnection	6	0.79	−85.27 (0)	99.83%	[0.80, 0.97]

4. Discussion

4.1. Longitudinal SDMT

SDMT scores in this population of early MS patients were significantly lower than control populations at both baseline and follow-up. There was a statistically significant increase in SDMT between the two time points that on average was greater than the 4-point MCID (mean 5.4 point increase). The observed increases in SDMT may be due to the fact that our cohort has just started treatment, presumably due to an acute worsening of symptoms, which then resolve over the interval from baseline to follow-up. Previous longitudinal studies of disease-modifying therapies in MS showed improvements in cognition (Mattioli et al., 2015). In particular, one study of SDMT reported an average gain of 15 points over 48 weeks (Morrow et al., 2010). We speculate that the bigger improvements in patients with lower baseline measures could either be regression to the mean, practice effects or it could be due to increased disease burden causing increased triggering of plasticity to initiate the brain's recovery mechanisms.

4.2. Lesion location, disconnection, and atrophy characterization

Global metrics of disconnection from the NeMo Tool did not show much difference from the normal population, and none of the global disconnection metrics were significant predictors of future SDMT. The lack of change in global metrics is likely due to the way they were calculated in the NeMo Tool. Only the streamlines passing through the lesions were removed from the connectome matrix, and this seemingly did not have a large impact at the global level. ChaCo scores showed that regions with the most disconnection were bilateral caudate, superior parietal gyri, caudal anterior cingulate, pericalcarine and putamen as found previously in patients that overlap with this cohort (Kuceyeski et al., 2015a). The most affected pairwise connections were between subcortical (caudate, putamen and thalamus), cingulate (posterior, caudal inferior and isthmus) and fronto-parietal regions (superior parietal and supramarginal gyri). In the JHU-MNI Eve Atlas, the regions with most overlap were all white matter structures, with the splenium, medial part (tapetum) and body of the corpus callosum, posterior thalamic radiation, posterior/superior corona radiata and superior fronto-occipital fasciculi the most affected. The tapetum were by far the most lesioned, which is not surprising as this white matter bundle in the corpus callosum traces the posterior periventricular area (Ge, 2006). The regional and region-pair disconnection are likely also partly due to the periventricular nature of MS lesions and the propensity for them to be located on the corpus callosum and white matter connecting to subcortical structures, including the thalamus.

4.3. Partial least squares regression results

The three disconnection models, atlas-overlap and GM atrophy model had moderate to high R^2. The demographics only model explained 35% of the variance in the data, with the best performing model (based on pairwise disconnection and GM atrophy) explaining 79% of the variance in the data. The Akaike weights strongly show that the pairwise disconnection/atrophy model, as opposed to that of atrophy and regional/global disconnection or atlas overlap, performed the best - its probability was 99.83% when compared to the others. Surprisingly, the GM atrophy model performed quite well, explaining 71% of the variance, despite the relatively low level of atrophy in these early MS patients. Previous works, although limited in number, have applied quantitative approaches to predict cognitive or motor scores in MS patients from demographics, MRI-based measures and other clinical information. Two recent studies 1) used various global MRI-based measures to predict cognitive efficiency (SDMT + PASAT) with an overall explained variance of 26.3% (Pinter et al., 2015) and 2) various regional measures of WM and GM pathology to predict SDMT with an explained variance of 31.7% (Artemiadis et al., 2018). These studies were cross-sectional, however, and cannot be directly compared to our longitudinal results that include baseline measures of SDMT, in addition to our various imaging metrics, in predicting follow-up SDMT. We can, however, estimate the amount of predictive accuracy that the different imaging metrics add to a model based on demographics only, which included baseline SDMT. In that case, 36% more variance is explained by including GM atrophy, 31% more for regional disconnection measures (ChaCo) and atrophy, 38% more for atlas overlap and atrophy and 44% more for pairwise disconnection measures and atrophy.

Our previous cross-sectional work relating baseline imaging metrics to baseline processing speed indicated GM atrophy in the right putamen were related to concurrent processing speed changes in early MS (Kuceyeski et al., 2015a). Here, we again show the importance of the right putamen's role in processing speed, as more atrophy in that structure was significantly predictive of worse follow-up SDMT in all four of the non-global models. Left putamen was also significantly predictive of follow-up SDMT in all the non-global models, except the pairwise disconnection model. Atrophy in the putamen has been detected in patients with MS, and some studies have detected relationships between putamen atrophy and motor and cognitive function. In particular, one study analyzed the relationships between cognitive scores and deep GM regions and found a significant relationship between atrophy in the putamen (and to a lesser extent, the thalamus) and SDMT measures (Batista et al., 2012). A study of atrophy in the putamen of relapsing-remitting MS patients found that it is more severely affected in the early stages of the disease (as the patient population here) than in the later stages (Krämer et al., 2015). The pairwise disconnection and atlas-overlap models also highlighted the significant contribution of atrophy in the cingulate, left fusiform gyrus and caudate nucleus, a structure which was found to have more atrophy in cognitively impaired versus cognitively preserved MS patients (Zhang et al., 2016). Increased longitudinal atrophy in the caudate was also found to significantly correlate with worsening SDMT scores (Loitfelder et al., 2014). Age and baseline SDMT were significant demographic predictors in all of the models, with, unsurprisingly, older age being associated with worse follow-up SDMT and higher baseline SDMT being associated with better follow-up SDMT.

Our previous cross-sectional work also indicated that T2-FLAIR abnormalities in WM connecting to parietal and occipital lobes, particularly areas related to visual processing, were related to worse SDMT scores. Generally, the model coefficients here indicated more baseline disconnection and lesion overlap with parietal, occipital, temporal and, to a lesser extent subcortical regions were significant predictors of worse future processing speed. In particular, the regional disconnection model highlighted the importance of connections to and from the right parahippocampal gyrus, a temporal region with key roles in visuospatial processing and episodic memory (Aminoff et al., 2013). The pairwise-disconnection model emphasized connections from right cuneus to right lateral occipital, right parstriangularis to right rostral middle frontal, right superior parietal to right lateral occipital gyrus, left lingual gyrus to left inferior temporal, right nucleus accumbens to right medial orbitofrontal and right rostral anterior cingulate. Generally, the pairwise disconnection model illustrated the importance of connections involving right parietal/occipital regions, right nucleus accumbens and left parietal and temporal regions, including the hippocampus whose primary role is memory. The atlas overlap model indicated the importance of lesions in the GM and WM of the occipital lobes, in particular the right precuneus - a central part of the default mode that has been shown to play a large role in cognitive impairments in MS. Also important in the atlas overlap model was the right cingulate and right posterior corona radiata, both of which were found to have more WM lesions in cognitively impaired versus cognitively preserved MS patients (Zhang et al., 2016). Because the 176-region JHU atlas and the 86-region atlas that the atrophy, global network metrics, ChaCo scores and pairwise disconnection scores are based on have varying anatomical delineations, it is somewhat difficult to compare the models directly. However, the comparison does allow some insight as to the sensitivity of the predictive models to different atlases.

4.4. Limitations

The NeMo Tool estimates the connectivity effects of WM abnormalities from a pathology mask coregistered to a database of 73 healthy control tractograms. WM connections vary in location and strength across the normal population - therefore the NeMo Tool's database may not precisely represent a given MS individual's connectivity patterns. We do, however, calculate average disconnection scores over 73 normal subjects to capture this variability. There may also be some errors in normalization of the WM abnormality masks to MNI space, particularly in MS patients whose anatomical scans may contain other pathologies as well as atrophy in GM. Normalization was checked visually for accuracy (see Supplemental Fig. 3 in Kuceyeski et al., 2015a for details); any small normalization error effects are again minimized by averaging disconnection values over 73 normal tractograms. Atrophy was also quite mild in this cohort (the largest mean z-score over the 86 regions was -0.78), as such, atrophy should have minimal impact on the normalization process. In MS patients with more advanced disease, more care would have to be taken to account for this atrophy when performing the normalization to MNI space, using, for example, multichannel registration (Roura et al., 2015). Within MS, there can also be diffuse damage in normal appearing white matter (Werring et al., 1999) that does not appear as a hyperintensity on T2-FLAIR and would not be identified with our methods. However, damage in normal appearing white matter in these early MS patients is likely minimal. In fact, our previous work with a largely overlapping set of MS patients showed only minor changes in their diffusion MRI summary statistics (fractional anisotropy and radial/mean diffusivity), which may be sensitive to pathology in normal appearing white matter (Cassol et al., 2004). The areas of diffusion MRI abnormality that we did identify largely overlapped with the areas in T2-FLAIR lesion masks (see Online Supplementary Fig. 3 in Kuceyeski et al., [2015]). Therefore, the effect of diffuse damage in normal appearing white matter on connectivity should be minimal in this cohort. Again, if one were to apply this model to MS subjects with more advanced disease, one may consider adding terms to the model to capture damage in normal appearing white matter. Finally, quantitative approaches that are data-driven improve in accuracy and stability with increasing amounts of data – here we use only a moderate sized-sample. Larger sample sizes would enable more thorough training/testing.

The SDMT is a test whose scores may be influenced by deficits in many different domains; it may depend on visual processing, memory and other cognitive domains that contribute to processing speed. We do not claim that our model is specific to any of these subdomains that contribute to the SDMT scores; it is merely reflective of the overall impairment captured by the SDMT. Future studies will attempt to collect more comprehensive cognitive and motor scores that would allow us to interrogate the specific regions that contribute to various elements of cognition or motor impairment. We believe that the general PLSR framework and input data presented here, with proper retraining of the PLSR model coefficients for each different outcome measure, could be used to create models (one per outcome measure) that would predict impairment in different domains as done previously (Kuceyeski et al., 2015b; Kuceyeski et al., 2016). This type of analysis allows comparison of the set of regions' metrics that are important to each outcome measure, akin to brain-behavior mapping.

4.5. Conclusion

We apply a quantitative approach to novel MRI-based metrics of lesion-induced disconnection in MS to predict future processing speed. We found that MS patients significantly improved in processing speed over time. Our model based on pairwise disconnection metrics and GM atrophy was able to predict with high accuracy future processing speed in MS patients. This model outperformed others based on regional/global disconnection and GM atrophy, GM atrophy only or atlas overlap metrics and GM atrophy. We also found that atrophy in the bilateral putamen, and white matter connectivity between occipital/parietal/temporal regions and subcortical structures was most influential in determining future processing speed in early MS patients. The overall goal of this work is to create a quantitative mapping tool for clinicians to use in creating accurate prognoses of future cognitive function for MS patients. Achieving this goal, however, will require collecting images, neuropsychological/physical impairment scores and demographic information from an extremely large number of patients at varying stages of the disease. The construction of such a large database will enable the application of machine learning approaches, which have the potential to shift the clinical management of complex neurological disorders like MS by helping physicians understand, diagnose, prognose and treat this heterogeneous and complicated disease. However, the success of these approaches hinges on the availability of large, public neuroimaging datasets that allow for through training and testing of prediction and model transparency that allows some physiological/clinical interpretation.

Acknowledgements

This work was supported by EMD Serono (SG), an Anna-Maria and Stephen Kellen Foundation Junior Faculty Fellowship (AK), and the NIH [CTSC grant UL1 TR000456-06 for database creation (SG), R21 NS104634-01 (AK) and R01 NS102646-01A1 (AK)]. The authors would like to acknowledge the help of Drs. Nancy Nealon, Jai Permumal and Timothy Vartanian at the Department of Neurology at Weill Cornell Medicine, New York, NY. The authors have no conflicts of interest to disclose.

Appendix A. Supplementary data

Supplementary data to this article can be found online at https://doi.org/10.1016/j.nicl.2018.05.003.

References

Aminoff, E.M., Kveraga, K., Bar, M., 2013. The role of the parahippocampal cortex in cognition. Trends Cogn. Sci. 17, 379–390.

Artemiadis, A., Anagnostouli, M., Zalonis, I., Chairopoulos, K., Triantafyllou, N., 2018. Structural MRI correlates of cognitive function in multiple sclerosis. Mult. Scler. Relat. Disord. 21, 1–8.

Bate, A.J., Mathias, J.L., Crawford, J.R., 2001. Performance on the Test of Everyday Attention and standard tests of attention following severe traumatic brain injury. Clin. Neuropsychol. 15, 405–422.

Batista, S., Zivadinov, R., Hoogs, M., Bergsland, N., Heininen-Brown, M., Dwyer, M.G., Weinstock-Guttman, B., Benedict, R.H.B., 2012. Basal ganglia, thalamus and neocortical atrophy predicting slowed cognitive processing in multiple sclerosis. J. Neurol. 259, 139–146.

Benedict, R.H., DeLuca, J., Phillips, G., LaRocca, N., Hudson, L.D., Rudick, R., Multiple Sclerosis Outcome Assessments Consortium MSOA, 2017. Validity of the Symbol Digit Modalities Test as a cognition performance outcome measure for multiple sclerosis. Mult. Scler. 23, 721–733.

Bergendal, G., Fredrikson, S., Almkvist, O., 2007. Selective decline in information processing in subgroups of multiple sclerosis: an 8-year longitudinal study. Eur. Neurol. 57, 193–202.

Bonferroni, C.E., 1936. Teoria statistica delle classi e calcolo delle probabilità. Pubbl del R Ist Super di Sci Econ e Commer di Firenze.

Burnham, K., Anderson, D., 2002. Model Selection and Multimodal Inference, 2nd ed. Springer-Verlag, New York, NY.

Cassol, E., Ranjeva, J.-P., Ibarrola, D., Mékies, C., Manelfe, C., Clanet, M., Berry, I., 2004. Diffusion tensor imaging in multiple sclerosis: a tool for monitoring changes in normal-appearing white matter. Mult. Scler. J. 10, 188–196.

Dale, A.M., Fischl, B., Sereno, M.I., 1999. Cortical surface-based analysis. I. Segmentation and surface reconstruction. NeuroImage 9, 179–194.

Efron, B., 1987. Better bootstrap confidence intervals. J. Am. Stat. Assoc. 82, 171–185.

Fischl, B., Sereno, M.I., Dale, A.M., 1999. Cortical surface-based analysis. II: inflation, flattening, and a surface-based coordinate system. NeuroImage 9, 195–207.

Ge, Y., 2006. Multiple sclerosis: the role of MR imaging. Am. J. Neuroradiol. 27.

Hu, B., Ye, B., Yang, Y., Zhu, K., Kang, Z., Kuang, S., Luo, L., Shan, H., 2011. Quantitative diffusion tensor deterministic and probabilistic fiber tractography in relapsing-remitting multiple sclerosis. Eur. J. Radiol. 79, 101–107.

Jones, D.K., Cercignani, M., 2010. Twenty-five pitfalls in the analysis of diffusion MRI data. NMR Biomed. 23, 803–820.

Krämer, J., Meuth, S., Tenberge, J.-G., Schiffler, P., Wiendl, H., Deppe, M., 2015. Early and Degressive putamen atrophy in multiple sclerosis. Int. J. Mol. Sci. 16, 23195–23209.

Krishnan, A., Williams, L.J., McIntosh, A.R., Abdi, H., 2011. Partial Least Squares (PLS) methods for neuroimaging: a tutorial and review. NeuroImage 56, 455–475.

Kuceyeski, A., Maruta, J., Niogi, S.N., Ghajar, J., Raj, A., 2011. The generation and validation of white matter connectivity importance maps. NeuroImage 58, 109–121.

Kuceyeski, A., Maruta, J., Relkin, N., Raj, A., 2013. The Network Modification (NeMo) Tool: elucidating the effect of white matter integrity changes on cortical and subcortical structural connectivity. Brain Connect. 3, 451–463.

Kuceyeski, A.F., Vargas, W., Dayan, M., Monohan, E., Blackwell, C., Raj, A., Fujimoto, K., Gauthier, S.A., 2015a. Modeling the relationship among gray matter atrophy, abnormalities in connecting white matter, and cognitive performance in early multiple sclerosis. Am. J. Neuroradiol. 36, 702–709.

Kuceyeski, A., Navi, B.B., Kamel, H., Relkin, N., Villanueva, M., Raj, A., Toglia, J., O'Dell, M., Iadecola, C., 2015b. Exploring the brain's structural connectome: a quantitative stroke lesion-dysfunction mapping study. Hum. Brain Mapp. 36, 2147–2160.

Kuceyeski, A., Navi, B.B., Kamel, H., Raj, A., Relkin, N., Toglia, J., Iadecola, C., O'Dell, M., 2016. Structural connectome disruption at baseline predicts 6-months post-stroke outcome. Hum. Brain Mapp. 37, 2587–2601.

LoCastro, E., Kuceyeski, A., Raj, A., 2014. Brainography: an atlas-independent surface and network rendering tool for neural connectivity visualization. Neuroinformatics 12, 355–359.

Loitfelder, M., Fazekas, F., Koschutnig, K., Fuchs, S., Petrovic, K., Ropele, S., Pichler, A., Jehna, M., Langkammer, C., Schmidt, R., Neuper, C., Enzinger, C., 2014. Brain activity changes in cognitive networks in relapsing-remitting multiple sclerosis – insights from a longitudinal fMRI study. Ed. Orhan Aktas. PLoS One 9, e93715.

Mattioli, F., Stampatori, C., Bellomi, F., Scarpazza, C., Capra, R., Rio, J., 2015. Natalizumab significantly improves cognitive impairment over three years in MS: pattern of disability progression and preliminary MRI findings. Ed. Ralf Andreas Linker. PLoS One 10, e0131803.

Mesaros, S., Rocca, M.A., Kacar, K., Kostic, J., Copetti, M., Stosic-Opincal, T., Preziosa, P., Sala, S., Riccitelli, G., Horsfield, M.A., Drulovic, J., Comi, G., Filippi, M., 2012. Diffusion tensor MRI tractography and cognitive impairment in multiple sclerosis. Neurology 78, 969–975.

Morrow, S., O'Connor, P., Polman, C., Goodman, A., Kappos, L., Lublin, F., Rudick, R., Jurgensen, S., Paes, D., Forrestal, F., Benedict, R., 2010. Evaluation of the symbol digit modalities test (SDMT) and MS neuropsychological screening questionnaire (MSNQ) in natalizumab-treated MS patients over 48 weeks. Mult. Scler. J. 16, 1385–1392.

Pagani, E., Bammer, R., Horsfield, M.A., Rovaris, M., Gass, A., Ciccarelli, O., Filippi, M., 2007. Diffusion MR imaging in multiple sclerosis: technical aspects and challenges. AJNR Am. J. Neuroradiol. 28, 411–420.

Pierpaoli, C., Barnett, A., Pajevic, S., Chen, R., Penix, L.R., Virta, A., Basser, P., 2001. Water diffusion changes in Wallerian degeneration and their dependence on white matter architecture. NeuroImage 13, 1174–1185.

Pinter, D., Khalil, M., Pichler, A., Langkammer, C., Ropele, S., Marschik, P.B., Fuchs, S., Fazekas, F., Enzinger, C., 2015. Predictive value of different conventional and non-conventional MRI-parameters for specific domains of cognitive function in multiple sclerosis. NeuroImage Clin. 7, 715–720.

Rocca, M.A., Valsasina, P., Martinelli, V., Misci, P., Falini, A., Comi, G., Filippi, M., 2012. Large-scale neuronal network dysfunction in relapsing-remitting multiple sclerosis. Neurology 79, 1449–1457.

Roura, E., Schneider, T., Modat, M., Daga, P., Muhlert, N., Chard, D., Ourselin, S., Lladó, X., Gandini Wheeler-Kingshott, C., 2015. Multi-channel registration of fractional anisotropy and T1-weighted images in the presence of atrophy: application to multiple sclerosis. Funct. Neurol. 30, 245–256.

Shu, N., Liu, Y., Li, K., Duan, Y., Wang, J., Yu, C., Dong, H., Ye, J., He, Y., 2011. Diffusion tensor tractography reveals disrupted topological efficiency in white matter structural networks in multiple sclerosis. Cereb. Cortex 21, 2565–2577.

Werring, D.J., Clark, C.A., Barker, G.J., Thompson, A.J., Miller, D.H., 1999. Diffusion tensor imaging of lesions and normal-appearing white matter in multiple sclerosis. Neurology 52, 1626–1632.

Wheeler-Kingshott, C.A.M., Cercignani, M., 2009. About “axial” and “radial” diffusivities. Magn. Reson. Med. 61, 1255–1260.

Yeo, B.T.T., Krienen, F.M., Sepulcre, J., Sabuncu, M.R., Lashkari, D., Hollinshead, M., Roffman, J.L., Smoller, J.W., Zöllei, L., Polimeni, J.R., Fischl, B., Liu, H., Buckner, R.L., 2011. The organization of the human cerebral cortex estimated by intrinsic functional connectivity. J. Neurophysiol. 106, 1125–1165.

Zhang, X., Zhang, F., Huang, D., Wu, L., Ma, L., Liu, H., Zhao, Y., Yu, S., Shi, J., 2016. Contribution of gray and white matter abnormalities to cognitive impairment in multiple sclerosis. Int. J. Mol. Sci. 18, 46.